

A Tumor-Targeted Nanodelivery System to Improve Early MRI Detection of Cancer

Kathleen F. Pirollo¹, John Dagata², Paul Wang³, Matthew Freedman¹, Andras Vladar², Stanley Fricke¹, Lilia Ileva¹, Qi Zhou¹, and Esther H. Chang¹

¹Georgetown University Medical Center, ²National Institute of Standards and Technology, and ³Howard University

Abstract

The development of improvements in magnetic resonance imaging (MRI) that would enhance sensitivity, leading to earlier detection of cancer and visualization of metastatic disease, is an area of intense exploration. We have devised a tumor-targeting, liposomal nanodelivery platform for use in gene medicine. This systemically administered nanocomplex has been shown to specifically and efficiently deliver both genes and oligonucleotides to primary and metastatic tumor cells, resulting in significant tumor growth inhibition and even tumor regression. Here we examine the effect on MRI of incorporating conventional MRI contrast agent Magnevist[®] into our anti-transferrin receptor single-chain antibody (TfRscFv) liposomal complex. Both in vitro and in an in vivo orthotopic mouse model of pancreatic cancer, we show increased resolution and image intensity with the complexed Magnevist[®]. Using advanced microscopy techniques (scanning electron microscopy and scanning probe microscopy), we also established that the Magnevist[®] is in fact encapsulated by the liposome in the complex and that the complex still retains its nanodimensional size. These results demonstrate that this TfRscFv–liposome–Magnevist[®] nanocomplex has the potential to become a useful tool in early cancer detection. *Mol Imaging* (2006) 5, 41–52.

Keywords: Nanocomplex, tumor targeting, Magnevist[®], MRI, early detection.

Introduction

The ability to detect cancer, both primary and metastatic disease, at an early stage would be a major step toward the goal of ending the pain and suffering from the disease. The development of tumor-targeted delivery systems for gene therapy has opened the potential for delivery of imaging agents more effectively than is currently achievable. Magnetic resonance imaging (MRI) can acquire 3-D anatomical images of organs. Coupling these with paramagnetic images results in the accurate localization of tumors as well as longitudinal and quantitative monitoring of tumor growth and angiogenesis [1,2].

One of the most common paramagnetic imaging agents used in cancer diagnostics is Magnevist[®] (gadopentetate dimeglumine). Gadolinium is a rare earth

element. It shows paramagnetic properties because its ion (Gd²⁺) has seven unpaired electrons. The contrast enhancement observed in MRI scans is due to the strong effect of Gd²⁺ primarily on the hydrogen-proton spin–lattice relaxation time (T1). Whereas free gadolinium is highly toxic and thus unsuitable for clinical use, chelation with diethylenetriamine pentacetic acid generates a well-tolerated, stable, strongly paramagnetic complex. This metal chelate is metabolically inert. However, after intravenous (iv) injection of gadopentetate dimeglumine, the meglumine ion dissociates from the hydrophobic gadopentetate, which is distributed only in the extracellular water. It cannot cross an intact blood–brain barrier and therefore does not accumulate in normal brain tissue, cysts, postoperative scars, etc, and it is rapidly excreted in the urine. It has a mean half-life of about 1.6 hr. Approximately 80% of the dose is excreted in the urine within 6 hr.

A systemically administered tumor-targeting delivery system has been developed in our laboratory for use in gene medicine [3–8]. This nanosized complex is composed of a cationic liposome encapsulating the nucleic acid payload, which can be either genes [3–6] or oligonucleotides [7,8]. Decorating the surface of the liposome is a targeting molecule that can be a ligand, such as folate or transferrin, or an antibody or an antibody fragment directed against a cell surface receptor. The presence of the ligand/antibody on the liposome facilitates the entry of the complex into the cells through binding of the targeting molecule by its receptor followed by internalization of the bound complex via receptor-mediated endocytosis, a highly efficient

Abbreviations: Lip, liposome; Mag, Magnevist[®] (Gadopentetate Dimeglumine); SEM, scanning electron microscopy; SPM, scanning probe microscopy; STEM, scanning transmission electron microscopy; TfRscFv, anti-transferrin receptor single chain antibody; TfRscFv-Lip-Mag, anti-transferrin receptor single chain antibody-liposome-Magnevist[®] complex.

Corresponding author: Esther H. Chang, PhD, Department of Oncology, Lombardi Comprehensive Cancer Center, Georgetown University Medical Center, 3970 Reservoir Road, NW, The Research Building, TRB E420, Washington, DC 20057-1460; e-mail: chang@georgetown.edu. Received 25 February 2005; Received in revised form 8 June 2005; Accepted 17 June 2005. DOI 10.2310/7290.2006.00005

internalization pathway [9,10]. This modification of the liposomes results in their being able to not only selectively deliver their payload to tumor cells, but also increases the transfection efficacy of the liposome. Transferrin receptor (TfR) levels are elevated in various types of cancer including oral, prostate, breast, and pancreas [11–16]. Moreover, the TfR recycles during internalization in rapidly developing cells such as cancer cells [16], thus contributing to the uptake of these transferrin-targeted nanocomplexes even in cancer cells where TfR levels are not elevated. The nanocomplex used in the studies described here uses an anti-transferrin receptor single-chain antibody fragment (TfRscFv) as the targeting moiety [17,18]. TfRscFv contains the complete antibody-binding site for the epitope of the TfR recognized by the monoclonal antibody 5E9 [18]. TfRscFv has advantages over the transferrin molecule itself, or an entire monoclonal antibody, in targeting liposomes to cancer cells with elevated TfR levels: (1) The size of the scFv (28 kDa) is much smaller than that of the transferrin molecule (80 kDa) or the parental monoclonal antibody (155 kDa). The scFv liposome–DNA complex may thus exhibit better penetration into small capillaries characteristic of solid tumors. (2) The smaller scFv has a practical advantage related to the scaled-up production necessary for the clinical trials. (3) The scFv is a recombinant molecule and not a blood product like transferrin and thus presents no danger of a potential contamination by blood-borne pathogens. (4) Without the Fc region of the monoclonal antibody, the issue of non-antigen-specific binding through Fc receptors is eliminated [19]. Most importantly, we have already shown that such an anti-TfR single-chain antibody molecule can target an intravenously administered cationic liposome–DNA nanocomplex preferentially to tumors [5,6]. Encapsulating Magnevist[®] within such a tumor-targeted nanocomplex offers potential advantages for enhanced sensitivity, detection of metastases, and diagnosis of cancer.

In this article, using a mouse xenograft model of human pancreatic cancer, we explore the use of this nanocomplex for systemic delivery of the imaging agent Magnevist[®] to tumors. In addition, we used scanning electron microscopy (SEM) and scanning probe microscopy (SPM) [20–25] to examine the physical structure and size of these Magnevist[®]-carrying nanocomplexes. Because gadolinium is a high-atomic-number element and possesses a large magnetic moment, these properties can be exploited in a variety of ways to enhance contrast in both SEM and SPM. The findings presented below demonstrate that our ligand–liposome nanocomplex does indeed encapsulate Magnevist[®] and that iv

administration of this complex results in enhanced tumor imaging.

Materials and Methods

Cell Lines

Human lymphoblastic leukemia cell line K562 was obtained from the Lombardi Comprehensive Cancer Center Tissue Culture core facility (Washington, DC). These suspension cells were maintained in RPMI 1640 supplemented with 10% heat-inactivated fetal bovine serum (FBS) plus 2 mM L-glutamine, and 50 µg/mL each of penicillin, streptomycin, and neomycin. Human pancreatic cancer cell line CaPan-1 (obtained from ATCC, Manassas, VA) was derived from a metastatic adenocarcinoma of the pancreas. It was maintained in Iscove's modified Dulbecco's medium containing 4 mM L-glutamine and sodium bicarbonate, supplemented with 20% non-heat-inactivated FBS, 2 mM L-glutamine, and 50 µg/mL each of penicillin, streptomycin, and neomycin. Human prostate cancer cell line DU145 (ATCC) was originally derived from a lesion in the brain of a patient with widespread metastatic carcinoma of the prostate. It was maintained in minimum essential medium with Earle's salts supplemented with 10% heat-inactivated FBS plus L-glutamine and antibiotics as above.

Nanocomplex Formation

Cationic liposome (DOTAP:DOPE) was prepared by the ethanol injection method as previously described [6]. When delivering plasmid DNA, the full complex was formed in a manner identical to that previously described [26]. To encapsulate the imaging agent, the TfRscFv was mixed with the liposome at a specific ratio (identical to that used with DNA) and incubated at room temperature for 10 min. Magnevist[®] was added to this solution, mixed, and again incubated at room temperature for 10 min. When stored at 2–8°C the complex is stable for at least 8 days, as determined by size measurements using a Malvern Zetasizer 3000H (Malvern, UK). The average of the cumulants (*Z* average) measurements over this time frame is 112.3 ± 4.67 (*SE*), whereas the polydispersity (representing the reproducibility of the values during repeat scans) is 0.445 ± 0.03 . For in vitro transfection, 2 mL of serum-free medium was added to the complex before transfection. When prepared for in vivo use, dextrose was added to a final concentration of 5%. For both in vitro and in vivo complex formation, the ratio of Magnevist[®] to liposome was 1:7 (vol/vol).

In Vitro Transfection

To transfect suspension cells K562, 15×10^6 cells in a total volume of 4.0 mL of medium with all supplements except serum (serum-free medium) were placed into a 100-mm² tissue-culture dish. Two milliliters of the transfection solution from above, containing varying amounts of Magnevist[®], was added to the cell suspension. The plate was incubated at 37°C with gentle rocking for the length of time given in the Results section (up to 90 min), after which the cells were gently pelleted ($600 \times g$ for 7 min) at 4°C in 0.5 mL microcentrifuge tubes and washed three times with 10 mL of serum free medium to remove any excess transfection solution and placed on wet ice until imaged.

In Vivo Tumor Targeting

To assess the tumor-selective targeting of the TfRscFv–liposome (TfRscFv–Lip) nanocomplex to primary and metastatic tumors, an orthotopic metastasis model using human pancreatic cancer cell line CaPan-1 was used. Subcutaneous xenograft tumors of CaPan-1 were induced in female athymic nude mice by injection of 1×10^7 CaPan-1 cells suspended in Matrigel collagen basement membrane matrix (BD Biosciences, San Jose, CA). Approximately 8 weeks later, the tumors were harvested and a single-cell suspension of the tumor was prepared. Cells ($1.2\text{--}1.5 \times 10^7$), also suspended in Matrigel were injected into the surgically exposed pancreas of female athymic nude mice as previously described [27]. Five weeks post surgery, the complex carrying the *LacZ* gene was iv injected $3 \times$ over 24 hrs (at 40 μg DNA per injection). Sixty hours later, the animals were sacrificed and examined for the presence of metastases and organs stained for β -galactosidase expression using a previously described procedure [3].

Magnetic Resonance Imaging

For in vitro MRI, the cell pellets in microcentrifuge tubes were positioned at the center of the magnet. The MRI was performed at Howard University using a 4.7-T horizontal bore NMR machine (Varian Inc, Palo Alto, CA). The imaging protocols consist of a multislice T1-weighted spin–echo imaging sequence and a saturation–recovery sequence. For the T1-weighted imaging technique, the repetition time (TR) was 1000 msec and the echo time (TE) was 13 msec. The T1-weighted spin–echo imaging technique was applied to verify the positive image enhancement. The saturation–recovery MR sequence with variable echo times was used for the T1 measurement. The slice thickness of images was 0.5 mm. The radiofrequency (RF) coil used was a 30-mm single-

loop coil. The RF coil serves as an RF transmitter and receiver. The RF pulse was a selective 5-msec sinc pulse. The number of phase-encoding steps was 256. The field of view was 15×15 mm. The image area chosen in the study was at the center of the RF coil for RF homogeneity. The MR images were taken in the cross-section direction of the microcentrifuge tube. The height of the cell pellet was 12 mm. The range of the multislice images covers the whole pellet. The center slice images, which were not influenced by the image distortion due to the susceptibility effect from the air–pellet boundary, were used for the studies. The image intensity was measured using the Varian Image Browser software. The signal is taken from a region of interest that is big enough to cover two thirds of the image from each microcentrifuge tube. The relative image intensities of the pellets from these tubes were applied for contrast enhancement evaluation and the T1 measurements.

For the in vivo studies, mice bearing CaPan-1 orthotopic tumors or DU145 subcutaneous xenograft tumors were used. The CaPan-1 tumors were induced as described above. DU145 tumors were induced by the subcutaneous inoculation of 7×10^6 cells in Matrigel. These studies were performed at Georgetown University. Animals to be imaged were anesthetized and placed in a proprietary, in-house designed, animal management system. This system incorporates a warm-water heating system that maintains the temperature at 37°C, as well as a four-channel, thermal optical monitoring system used to monitor animals' skin temperature, ambient temperature, and wall temperature of the device. For imaging, anesthesia was induced using isoflurane at 4%, with the remaining gas composed of a 66% oxygen and 30% nitrous oxide mixture. Maintenance of anesthesia was achieved with 1.5% isoflurane under similar gaseous conditions of oxygen and nitrous oxide as noted. The anesthetized animal was positioned inside a cylindrical, variable RF resonant antenna (birdcage resonator volume coil) and tuned to a center frequency of approximately 300 MHz (the resonant frequency of water molecules when subject to a field strength of 7 T). The imaging protocol used was T1-weighted Turbo-RARE (rapid acquisition with rapid enhancement) 3-D imaging sequences performed on a 7T Bruker BioSpin (Billerica, MA) imaging console. The imaging parameters used were as follows: T1-weighted Turbo-RARE 3-D, TE 13.3 msec, TR 229.5 sec, flipback on, four echoes with a field of view of 8.0/3.5/3.5 cm and a $256 \times 256 \times 256$ matrix. After a baseline image was acquired, the animal was kept immobilized in the animal holder and the Magnevist[®] only [diluted to 400 μL with $1 \times$ phosphate-

buffered saline (pH = 7.4)] or the TfRscFv–Lip–Mag complex (total volume 400 μ L) was systemically administered using a 27 G needle by iv injection into the tail vein of the animal and the 3-D imaging sequence was immediately initiated. The imaging with the two solutions were performed on sequential days.

Scanning Electron Microscopy

Sample solutions of liposome-encapsulated Magnevist contrast agent and complete nanocomplex consisting of a tumor-targeting single-chain transferrin receptor protein coating the liposome-encapsulated complex, TfRscFv–Lip–Mag, were prepared at Georgetown University Medical Center (GUMC), delivered to National Institute of Standards and Technology (NIST) and were stored under dark and refrigeration. For each imaging session, a fresh dilution 1:3 by volume with deionized water was prepared and a 5- μ L droplet was micropipetted onto a standard 200-mesh transmission electron microscopy grid consisting of 30–60 nm formvar and 15–20 nm carbon. The droplet was allowed to dry on the grid in air for 5 min before being loaded into the vacuum chamber of the microscope. Imaging was performed using a Hitachi S-4800 field-emission microscope at NIST. Of particular interest to applications of SEM to nanocomplex imaging is a comparison of upper and lower secondary electron detectors [SE9(U) and SE(L)]—using the SEM in its usual mode—to the addition of a transmitted electron (TE) detector, transforming the instrument into a low-voltage STEM.

Scanning Probe Microscopy

Sample solutions of liposome-encapsulated Magnevist contrast agent and complete nanocomplex were prepared at GUMC, delivered to NIST, and were stored under dark and refrigeration. For each imaging session, a fresh dilution 1:3 by volume with deionized water was prepared and a 5- μ L droplet was micropipetted onto an ultrasonically cleaned silicon substrate used with native oxide or with a poly-L-lysine coating. SPM imaging were obtained using a Veeco (Santa Barbara, CA) MultiMode microscope with a Nanoscope IV controller. Topography by tapping mode with Z control [Veeco RTESP cantilevers, of approximately 320–360 kHz and k approximately 20–60 N/m], phase imaging, and magnetic force microscopy using magnetic-coated tips (Veeco MESP 68 kHz) were performed in life mode. Dynamic imaging of dewetting and surface energy “phase separation” as the solution evaporates to expose isolated nanoparticles and aggregates were used to understand the consequences of solvent drying on the stability of the particles

and its effect on the various SPM contrast mechanisms available with the SPM system.

Results

Tumor-Specific Targeting by the Ligand–Liposome Nanocomplex Carrying a Reporter Gene

To assess selective targeting of the TfRscFv–LipA nanocomplex to primary tumor and metastases, an orthotopic metastasis model, a closer approximation of the clinical situation, using human PanCa cell line CaPan-1 was used. Surgical orthotopic implantations of CaPan-1 xenograft tumor sections into nude mice have been shown to produce, within 56 days, metastases in liver and spleen [27]. Orthotopic tumors of CaPan-1 were induced in female athymic nude mice as described in Materials and Methods. Approximately 5 weeks later, the animals were euthanized and necropsied to look for tumor in the pancreas and other organs. As shown in Figure 1A, extensive tumor growth is evident throughout the pancreas. Metastases were present in various organs in four of five mice including the spleen, liver, lung, adrenal gland and even within the diaphragm. This experiment was repeated with similar results.

To establish selective targeting tumor and metastasis, before sacrificing the mice, the TfRscFv–LipA complex carrying pSVb (LacZ) plasmid DNA for β -galactosidase expression was iv injected into the mice three times over a 24-hr period (40 μ g of plasmid DNA per injection). All five mice were sacrificed 60 hr after injection and various organs, including the liver, lung, spleen, pancreas and

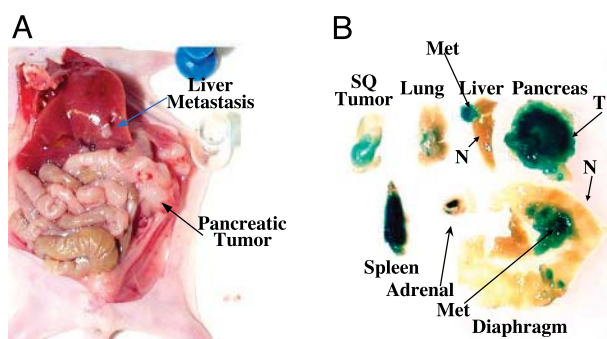


Figure 1. Tumor-specific targeting of a CaPan-1 orthotopic metastasis model by the TfRscFv–Lip–DNA nanocomplex. Subcutaneous CaPan-1 xenograft tumors were induced in female athymic nude mice as described in Materials and Methods. The tumors were harvested and a single-cell suspension in Matrigel was injected into the surgically exposed pancreas. Five weeks post injection, the TfRscFv–Lip complex carrying the LacZ gene for β -galactosidase expression (40 μ g) was iv injected 3 \times over 24 hr. Sixty hours later, the animals were sacrificed and examined for the presence of metastases and the organs stained for β -galactosidase expression. The same tumor nodule in the liver indicated by an arrow in A exhibits intense β -galactosidase expression in B. (A) Gross necropsy; (B) tissues after staining for β -galactosidase.

diaphragm, were harvested and examined for the presence of metastasis and tumor-specific staining. Fresh samples, sliced at 1-mm thickness, were stained with X-gal to produce a blue color where the gene is expressed. The tumor-targeting ability and high transfection efficiency of the complex is demonstrated by the presence of the reporter gene in the various organs from this animal (Figure 1B). In the liver, lung, adrenal gland, and diaphragm, it is clearly shown that the reporter gene is highly expressed only in the metastases, whereas in the adjacent normal tissue, no blue color is evident. The metastasis visible in the liver in Figure 1A (arrow) is the same tumor nodule strongly expressing β -galactosidase in Figure 1B (arrow) confirming the tumor-specific nature of this nanocomplex. In some of the mice, growth of the tumor in pancreas also resulted in extrusion of tumor through the original incision site used for implantation. In Figure 1B, this strongly blue stained subcutaneous tumor, surrounded by normal nonstained skin, is also shown, again showing tumor cell specificity. Similar results were observed in the rest of the mice and in the repeat experiment. Thus, this systemically administered nanocomplex will target tumor cells, both primary and metastatic, wherever they occur in the body, and efficiently deliver plasmid DNA. We wished to expand the potential of this delivery system to include contrast agents. The ability to do so could result in improved imaging and cancer detection.

In Vitro Studies Using TfRscFv-Lip Complex to Deliver Magnevist[®]

As Magnevist[®] is one of the most frequently used contrast agents in the clinic, it was chosen for use in these studies. In our initial experiments, we examined whether the complex could be prepared with Magnevist[®] and if doing so would enhance the MRI signal. Because trypsinization could lead to membrane damage and leakage of contrast agent from the cells, adherent cells were not used in these studies. Instead, a human lymphoblastic leukemia cell line, K562, which grows as a suspension culture was used. Moreover, gentle pelleting and washing of the cells would remove any excess Magnevist[®] or complex before imaging, allowing only cell-associated signal to be detected.

Time-Dependent Image Enhancement by the TfRscFv-Lip-Mag Nanocomplex

We examined the optimal time for transfection of the TfRscFv-Lip-Mag nanocomplex. The suggested clinical dose of Magnevist is 0.1 mmol/kg. In these initial studies, we used a dose of 0.3 mmol/kg (corrected for the smaller weight and blood volume of mouse vs. man)

in the complex per 250 μ L of transfection solution. K562 cells were transfected for times ranging from 20 to 90 min. Twenty minutes showed very low transfection activity based on the image intensity (data not shown). However, as shown in Figure 2A, by 60 min the cells transfected with the complex showed a large increase in intensity as compared to the untreated cells. The intensity of the untreated cells (202 ± 48) was not significantly different from that of an empty marker tube (194 ± 43), indicating that the cells themselves do not contribute to the signal detected. More importantly, the transfection efficiency plateaus at approximately 60 min because the relative intensity of the cells transfected for 60 and 90 min were identical (317 ± 46 and 317 ± 47 , respectively).

Magnevist[®] Dose-Dependent Image Enhancement

Using 60 min as the transfection time, we then assessed the effect of increasing amounts of Magnevist[®] on the TfRscFv-Lip-Mag complex image enhancement. The doses tested were 0.05, 0.3, and 0.9 mmol/kg. Corrected for size and blood volume of the mouse, the volumes of Magnevist[®] used in the complex per 250 μ L of transfection solution were 0.25, 1.5, and 4.5 μ L. As shown in Figure 2B and Table 1, the image intensity increases and the T1 relaxation time shortens as a function of the amount of contrast agent included in the complex.

Image Enhancement by TfRscFv-Lip-Mag as Compared to Free Magnevist[®]

Based on the above experiments it appears that the TfRscFv-Lip can complex with Magnevist[®] and deliver it to the cells for image enhancement. To assess the level of enhancement of the complexed contrast agent as compared to the agent alone and demonstrate that the signal obtained is not due to the presence of unincorporated Magnevist[®], we treated K562 cells with either free Magnevist[®] or the TfRscFv-Lip-Mag nanocomplex. The identical amount of contrast agent (0.3 mmole/kg or 1.5 μ L/250 μ L transfection volume) and transfection time (60 min) was used for both solutions. Whereas free Magnevist[®] showed enhanced contrast relative to the untreated cells as expected, the cells treated with the TfRscFv-Lip-Magnevist complex demonstrated a much greater increase in image intensity and shortened T1 relaxation time compared to both untreated and free-Magnevist[®]-treated cells (Figure 2C, Table 2). These results not only demonstrate the increased efficiency of contrast agent uptake by means of the targeted nanocomplex, but also indicate that the observed signal is

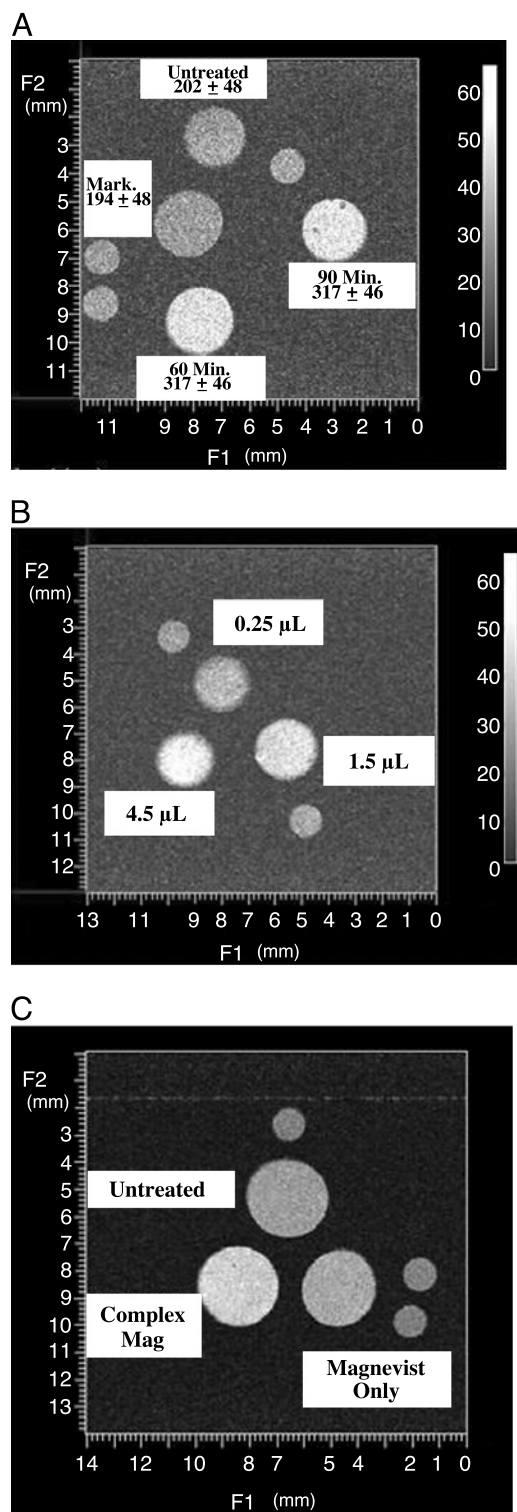


Figure 2. *In vitro* MRI of K564 cells after transfection with the TfRscFv–Lip–Mag nanocomplex. After transfection with either free Magnevist[®] or the noncomplex encapsulating Magnevist[®] the cells were pelleted and washed with serum-free medium, and MRI performed using a 4.7T Varian NMR. The imaging protocol consisted of T1-weighted spin–echo imaging sequences (TR/TE, 1000/13 msec) to verify the image enhancement and a saturation–recovery MR sequence with variable echo times for the T1 measurement. (A) Time-dependent transfection. The values given are relative intensities. (B) Variation in relative intensity with the amount of Magnevist[®] included in the complex (in microliters). (C) Comparison of relative intensity of the TfRscFv–Lip–Mag complex versus free Magnevist[®]. The small circles in all images are markers for sample orientation.

Table 1. Relative Intensity and T1 Relaxation Time as a Function of Magnevist[®] in the Complex

Dose of Contrast Agent (mM/kg)	Relative Intensity	T1 (sec)
0.05 (0.25 µL)	293 ± 50	1.43 ± 0.007
0.3 (1.5 µL)	379 ± 43	1.16 ± 0.004
0.9 (4.5 µL)	454 ± 51	1.01 ± 0.004

likely not due to uncomplexed Magnevist[®]. Further evidence of Magnevist[®] encapsulation is given below.

In Vivo Image Enhancement with TfRscFv–Lip–Mag

The above studies established that the nanocomplex could more efficiently image tumor cells *in vitro* than Magnevist[®] alone. However, to have potential for clinical use, the complex must exhibit a similar effect *in vivo*. We used the same human pancreatic cancer orthotopic mouse model (CaPan-1) for these studies as was used above to demonstrate tumor-specific targeting of the complex carrying a reporter gene. In addition, a second tumor model, a subcutaneous prostate xenograft mouse model (DU145) was also used. Mice bearing CaPan-1 or DU145 tumors were imaged on a 7T Bruker NMR as described in Materials and Methods. Once positioned in the coil, a baseline image was obtained using a T1-weighted Turbo-RARE 3-D imaging sequence. To facilitate image alignment, after baseline acquisition the animal was maintained in the animal holder while the imaging solution was administered via iv injection. Signal acquisition was begun within 3 min of the injection. The amount of Magnevist[®] administered to the mouse, either free (as is performed in the clinic) or included in the complex, was 10 µL. This amount is equivalent to 0.2 mmole/kg or twice that used in humans. This amount was selected because the standard human dose of 0.1 mmole/kg Magnevist[®] alone gave a very poor signal in the mice. The imaging with free Magnevist[®] and the TfRscFv–Lip–Mag complex were performed on two consecutive days. A baseline scan was also performed before administration of nanocomplex to confirm that all of the Magnevist[®] from the previous day had been washed out. MR technique and windows were consistent between the two sets of images with the windows

Table 2. Comparison of the Relative Intensity and T1 Relaxation Time between Free and Complexed Magnevist[®]

Treatment	Relative Intensity	T1 (sec)
Untreated	455 ± 47	1.80 ± 0.009
Free Magnevist [®]	538 ± 50	1.51 ± 0.007
Complexed Magnevist [®]	662 ± 52	1.40 ± 0.004

adjusted to correct for an automatic windowing feature of the scanner.

Images of the Magnevist[®] and nanocomplex–Magnevist in three separate mice are shown in Figure 3. In Figure 3A, 4 months after surgical implantation of the CaPan-1 tumor cells, the animal is carrying a large orthotopic tumor. The increased resolution and signal intensity, as compared to the contrast agent alone is quite evident. Similar results are observed in the second mouse with a CaPan-1 tumor shown in Figure 3B. This animal, only 2 months postsurgery, has a visible subcutaneous tumor growing through the site of the incision. A small abdominal mass was also detected by palpation. Not only is the signal in the subcutaneous tumor more enhanced after administration of the complexed Magnevist[®], but what appears to be the small orthotopic tumor (arrow) is evident in this scan and not in the one in which the animal received the free Magnevist[®]. Similarly, increased definition and contrast are evident in the subcutaneous DU145 tumor (Figure 3C) after

injection with the TfRscFv–Lip–Mag complex as compared to the free Magnevist[®]. Reconstruction and quantitation was performed on the images in Figure 3B and C, representing the two different tumor models, pancreatic cancer (CaPan-1) and prostate cancer (DU145). In both instances, there is an increased intensity (pixels) by the free Magnevist[®] over the baseline, as expected (Table 3). However, delivery of the imaging agent by the tumor-targeting nanocomplex results in an almost three-fold further increase in signal intensity in both of these tumor models. These studies thus demonstrate that when Magnevist[®] is incorporated within the TfRscFv–Lip complex there is an improved tumor visualization in an *in vivo* situation, and they suggest the potential benefit of further developing this means of tumor detection for clinical use.

Physical Characterization Studies

Whereas the *in vitro* studies offered circumstantial evidence that complexed Magnevist[®] is encapsulated

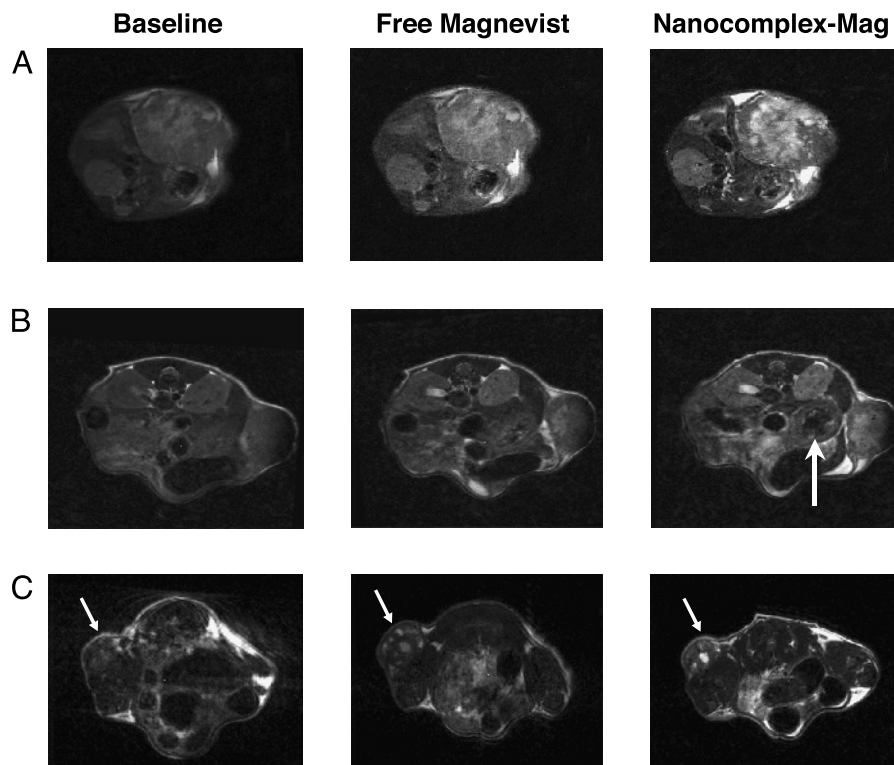


Figure 3. Improved MRI in two different models of cancer using the ligand–liposome–Mag nanocomplex. Human pancreatic cancer cells (CaPan-1) were surgically implanted into the body of the pancreas, and human prostate cancer cells (DU145) were subcutaneously injected on the lower back of female athymic nude mice. Free Magnevist[®] or the TfRscFv–Lip nanocomplex containing the same dose of Magnevist[®] was *iv* injected (via the tail vein) into each of the three mice on two consecutive days. This amount of Magnevist[®] is equivalent to twice the dose that would be administered to a human patient. The total volume of solution administered in all cases was 400 μ L. A baseline scan was performed just before administration of the nanocomplex to confirm that all of the Magnevist[®] from the previous day had been washed out. MR technique and windows were constant between the three sets of images, with the windows adjusted to correct for an automatic windowing feature of the scanner. (A) Differences in MRI signal in a large pancreatic orthotopic tumor (arrow) (4 months after surgical implantation of the tumor) between the *iv*-administered free contrast agent and the TfRscFv–Lip–Mag complex. (B) Similar effect in a second mouse with a subcutaneous pancreatic tumor and a much smaller abdominal pancreatic tumor (arrows). (C) Images of a third animal with a subcutaneous prostate tumor (arrow) in which the same effect is evident.

Table 3. Intensity Increase over Baseline by Free and Complexed Magnevist[®]

	CaPan-1	DU145
	% Increase over Baseline	
Complexed Magnevist [®]	99	215
Free Magnevist [®]	34.5	70

within the liposome, we have used sophisticated microscopy techniques (SEM and SPM) to confirm this fact and further characterize (e.g., complex size) the TfRscFv–Lip–Mag complex.

Imaging of Liposomes without Magnevist. High-resolution imaging implies narrow depth of focus and so requires relatively thin and flat samples. How thin varies with technique, but surface and substrate effects—surface energy and symmetry lowering—often dominate the structural forces typical of biomaterials. This is particularly true for liposomes given their tenuous nature [28]. So an understanding of reliable methods for preparing and characterizing the dimensional and mechanical stability of isolated liposomes is an essential step. The goal of our present characterization efforts is to perform direct sensing of the mechanical stiffness and magnetic properties of nanoparticles to establish that the contrast agent is indeed contained within the nanoparticle and not simply associated externally with the liposomes.

The SPM images surface topography in tapping mode by oscillating the tip and cantilever to which it is attached close to the cantilever resonance frequency. A feedback circuit maintains the oscillation of the cantilever at constant amplitude. This constant amplitude is given by a set point that is somewhat smaller than that of the freely oscillating cantilever. Because the SPM tip interacts with the surface through various small forces, there is a phase shift between the cantilever excitation and its response at a given point on the surface. For an inhomogeneous surface, the tip–surface interactions will vary according to surface charge, steep topographical changes, and mechanical stiffness variations, for example. By changing the set point and observing how certain features respond to softer or harder tapping, we can correlate this with the response expected for a specific structure such as a liposome. (The free oscillation amplitude signal is approximately 1.78 V.) A sequence of SPM phase images of a pair of isolated liposomes without payload is shown in Figure 4. Figure 4A was imaged at a set point of 1.68 V and the corresponding negative phase difference between the substrate and liposome indicates that the tip–sample

interaction is attractive for the liposome, given by a phase value of -3.5° . In the case of an attractive interaction and negative phase, the phase image of the liposome appears dark, except for a topographically keyed ring at the liposome edge. Figure 4B demonstrates the effect of reducing the set point to 1.45 V: The liposome now appears bright because the tip–sample interaction becomes repulsive, and here the phase difference between the liposome and substrate is $+8^\circ$. Finally, Figure 4C shows that the phase difference recorded at a set point of 1.35 V increases further, becoming $+35^\circ$.

Imaging of Liposome-Encapsulated Magnevist. Figure 5 presents SPM and SEM images of isolated lipo-

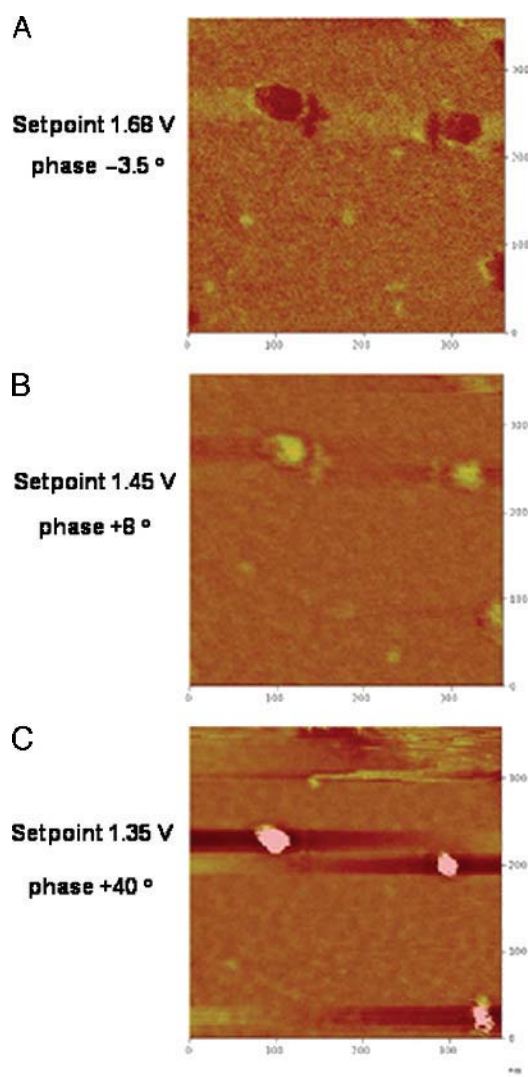


Figure 4. SPM phase images of liposomes without Magnevist[®]. The images appearing in A, B, and C were obtained at set points of 1.68, 1.45, and 1.35 V, respectively. The corresponding phase differences between the noncompliant substrate and the mechanically compliant liposome are -3.5° , $+8^\circ$, and $+40^\circ$. The interaction of the SPM tip and liposome changes from attractive to repulsive as the set point is decreased.

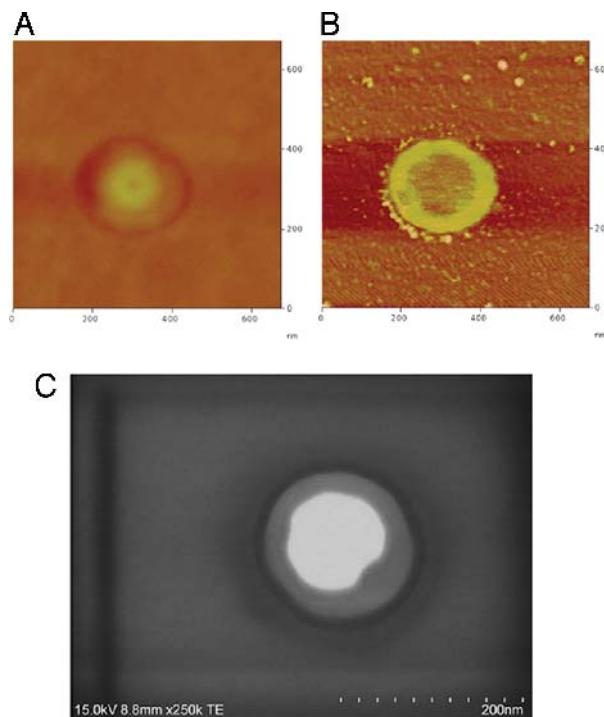


Figure 5. SPM and SEM images of liposome-encapsulated Magnevist[®] (Lip+Mag). (A) Atomic force microscopy topographical image of the liposome-encapsulated Magnevist[®] particle. The SPM phase image (set point = 1.6) (B) and 15 keV SEM (TE) (transmission-mode electron detector) image (C) possess similar contrast, although generated by entirely distinct complementary physical mechanisms.

some-encapsulated Magnevist (Lip+Mag) nanoparticles. The size distribution of single (Lip+Mag) particles is in the diameter range of 100–200 nm and scales according to optical measurements that indicate that payload-encapsulating liposomes are approximately 50% larger than liposomes alone in their spherical state.

The SPM topograph in Figure 5A indicates that liposomes containing Magnevist have a bimodal surface shape after drying that is more complex than that of the simple elliptical surface of a liposome containing no payload (not shown). The SPM phase behavior differs markedly from that of payloadless liposomes, the outer ring is repulsive relative to the center, and a corresponding SPM phase image is shown in Figure 5B. Regions of both attractive and repulsive tip–sample interaction appear at moderate set point values. A correlation between the SPM phase image obtained at a set point of 1.6 and the SEM image in TE mode is evident in Figure 5B and C. Liposomes appear uniformly bright across the entire particle in SEM images (not shown), similar to the uniform phase images we obtain by SPM. Tips and cantilevers change with time and usage. Moreover, it is important to verify that the images produced are not affected by tip instabilities due to

foreign material on the tip. Thus, they are changed frequently. Because each cantilever is somewhat different with respect to its resonance properties, the set points used in Figures 4 and 5 are different.

Imaging of TfRscFv–Lip–Mag Nanocomplex. The complete TfRscFv–Lip–Mag nanocomplex was prepared and imaged by SEM and SPM as described in Materials and Methods. Results, shown in Figure 6 indicate that the solvent film undergoes phase separation; however, examples of isolated NDS can be readily observed on the dried film. Note that the SEM beam clearly causes some damage to the film, but the particles can be repeatedly scanned several times before beam damage becomes significant. The appearance of the full complex is different from that of the (Lip+Mag) only. The shape is less regular and considerable texturing of the liposome surface following drying is consistent with protein denaturation. Also, SEM TE images indicate that the well-defined boundary between the outer ring and center of the liposome seen with the (Lip+Mag) particles is less

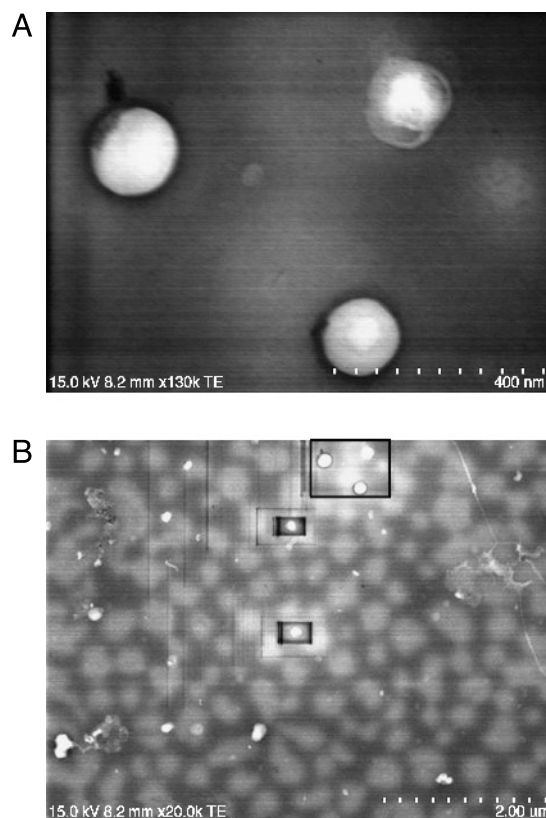


Figure 6. SPM topographic and phase imaging of TfRscFv–Lip–Mag nanocomplex. (A) 15 keV SEM (TE) (transmission-mode electron detector) image of the full nanocomplex. A suitable choice of amplitude set point readily distinguishes intact nanocomplex particles from decomposition products. It is not known if the decomposed material was present in the solution before sample preparation or is the direct result of interaction with the substrate. (B) power image of the field. The boxed area is the image in A.

apparent and the shape much more variable. This is consistent with the view that the presence of protein within the liposome has altered the osmotic outflow across the liposome during film drying.

It is possible to obtain additional information about these NDS particles by using the magnetic force microscopy imaging capabilities of the SPM (MFM). Because the magnetic moment of gadolinium-containing Magnevist is quite large, it should be possible using a magnetized SPM tip to interact with the oriented Magnevist concentrated within the liposomes. This is shown in Figure 7 for MFM of several approximately 100- to 200-nm-diameter nanocomplexes. We establish that, in fact, we are producing an image that is truly magnetic in nature by using the lift-mode capabilities of the SPM: In this mode, a topographic image under normal tapping

mode conditions is obtained. The reference surface information is then used to offset the tip by a specified height away from the surface and the surface is then scanned at this increased height. This removes the influence of topography on the signal. MFM images obtained in lift mode at a height of 15 nm or more from the surface are given by the magnetic phase image. The appearance of a signal confirms the presence of gadolinium encapsulated within the complex.

Discussion

The development of nanoparticle-sized delivery systems that have greater tumor and tissue penetrance is a major direction in medical research in general and cancer research in particular. Combining the capabilities of these small particles with the ability to home specifically to tumor cells wherever they occur in the body could lead to significant advances in cancer treatment and diagnosis. We have previously shown that our ligand-liposome-DNA complex can specifically target and efficiently transfect tumor cells (primary and metastatic) [3–8]. When encapsulating plasmid DNA, this targeted delivery system is truly a nanocomplex, with a uniform size of less than 100 nm [29]. Used in combination with conventional radiation/chemotherapy, delivery of therapeutic genes such as wild-type p53 by means of this nanodelivery system has resulted in tumor growth inhibition and even tumor regression in animal models [3–5,29]. This tumor regression and concomitant decrease in blood flow due to p53-mediated antiangiogenesis have also been demonstrated using Power Doppler ultrasound imaging [30]. Adapting such a tumor-targeted nanocomplex to deliver imaging agents would have the potential to improve early diagnosis as well as detection of metastatic disease. The results described above demonstrate that we can encapsulate and deliver the commonly used MRI agent Magnevist[®] to tumor cells both in vitro and in an orthotopic animal model and in doing so produce a more defined and intense image than seen with uncomplexed Magnevist[®].

Other nanometer-sized delivery systems for contrast agents are being developed. A chylomicron-remnant-like vehicle of approximately 90 nm containing polyiodinated triglyceride analogs in a neutral lipid core has been developed as a hepatocyte-selective contrast agent for computed tomography in animals [31]. A paramagnetic liquid perfluorocarbon nanoparticle of approximately 250 nm to which an anti- $\alpha_v\beta_3$ antibody has been conjugated is being developed for MRI to assess angiogenesis and atherosclerosis [32,33]. However,

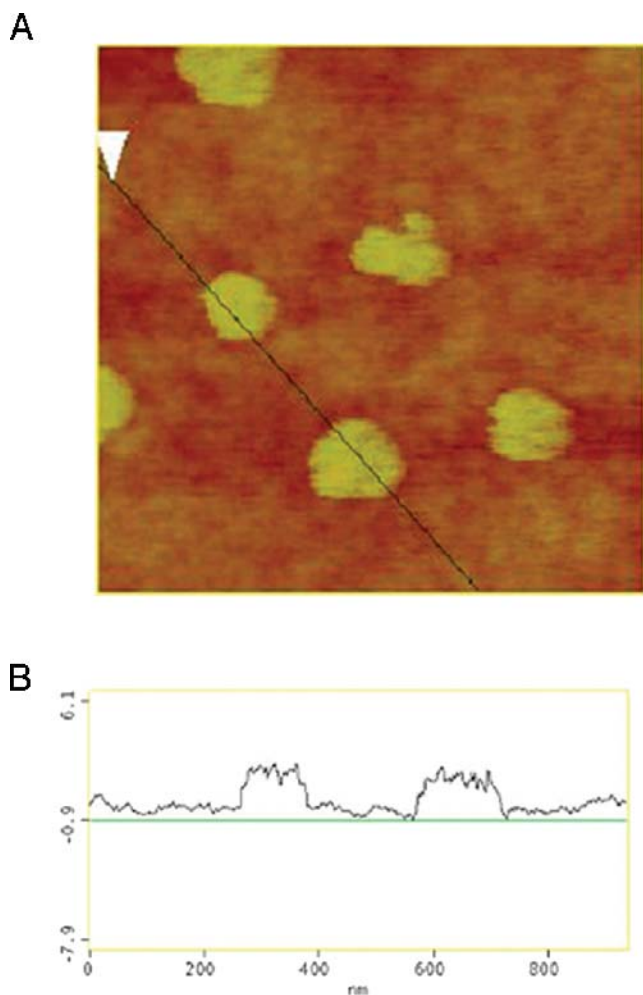


Figure 7. Cross-sectional comparison of SPM topographic and magnetic phase image in lift mode using 25-nm height displacement. (A) SPM topographic/magnetic phase image of the full TfRscFv-Lip-Mag nanocomplex. The appearance of a double dipole-like signal in B consisting of attractive and repulsive in-plane magnetic interactions suggests that the cause of this interaction is the nonuniform toroidal distribution of Magnevist within the NDS, consistent with SEM and nonmagnetic SPM phase images.

none of these are tumor targeting or currently applicable for cancer. However, given, as shown in Figure 1, that our nanocomplex can target metastatic disease it is anticipated that use of the nanocomplexed Magnevist® would also enhance detection sensitivity for metastases. The results shown here are with primary tumors. Studies are currently under way to compare the sensitivity of detection between free Magnevist® and the TfRscFv–Lip–Mag complex in metastases.

Using SEM and SPM we have also shown that the TfRscFv–Lip complex maintains its nanometer size when Magnevist® is encapsulated (particles of approximately 100–200 nm are shown in Figures 6 and 7). We have also demonstrated that the structural and mechanical properties of liposomes containing a payload are sufficiently different from those without one for it to be possible to confirm that Magnevist® is indeed encapsulated with the liposome. This was further confirmed by MFM imaging of the complex.

A tentative explanation for the internal structure of (Lip+Mag) is that the slight bulge in the SPM topographic image, represents a liposome-confined phase separation, that is, formation of a dense Magnevist–lipid toroidal distribution around the periphery of the particle with a preferential aqueous phase at the particle's center. This response is probably attributable to several important factors: First, the properties of Magnevist solution are pH approximately 6.5–8, an osmolality of 1,960, and viscosity of 4.9 at 20°C according to the manufacturer. A plausible chemical basis for this separation of the solution noted in the Magnevist data sheet: The meglumine salts dissociate completely from the complex, so changes in the local osmotic conditions. Coupled with the charge interaction of the gadolinium complex and cationic lipid, these interactions may provide a strong driving force for a hypertonic phase separation within the liposome. The charge distribution between the cationic lipid and Magnevist solution is effective at stabilizing the liposome and at providing structural support in solution and apparently in the bloodstream. This enhanced structural support is an important benefit for our studies because it enables most particles to remain intact during the film-drying process, in contrast to the extensive decomposition observed with the liposome-only solutions.

Therefore, we have been able to successfully encapsulate an MR contrast agent in our tumor-targeted nanodelivery system. The image enhancement demonstrated by the complex over conventionally delivered Magnevist® indicates the potential of this system to improve early detection of cancer via MRI.

Acknowledgments

We thank Ms. Brianna Kalk, Ms. Angelique Forrester, and Mr. Luis Torres for assistance in preparation of this manuscript, as well as the LCCC Animal Research Resource and Tissue Culture Shared Resource Facilities for their assistance in these studies. This work was supported in part by grants from NCI (CA103579-01) and SynerGene Therapeutics Inc (to K. F. P.) and from NFCR (to E. H. C.).

References

- [1] Gillies RJ, Bhujwala ZM, Evelhoch J, Garwood M, Neeman M, Robinson SP, Sotak CH, Van Der SB (2000). Applications of magnetic resonance in model systems: Tumor biology and physiology. *Neoplasia*. **2**:139–151.
- [2] Degani H, Chetrit-Dadiani M, Bogin L, Furman-Haran E (2003). Magnetic resonance imaging of tumor vasculature. *Thromb Haemost*. **89**:25–33.
- [3] Xu L, Pirolo K, Tang W, Rait A, Chang EH (1999). Transferrin–liposome-mediated systemic p53 gene therapy in combination with radiation results in regression of human head and neck cancer xenografts. *Hum Gene Ther*. **10**:2941–2952.
- [4] Xu L, Pirolo K, Chang EH, Murray A (1999). Systemic p53 gene therapy in combination with radiation results in human tumor regression. *Tumor Targeting* **4**:92–104.
- [5] Xu L, Tang WH, Huang CC, Alexander W, Xiang LM, Pirolo KF, Rait A, Chang EH (2001). Systemic p53 gene therapy of cancer with immunoliposomes targeted by anti-transferrin receptor scFv. *Mol Med*. **7**:723–734.
- [6] Xu L, Huang C-C, Huang W-Q, Tang W-H, Rait A, Yin Y, Cruz I, Xiang L-M, Pirolo K, Chang EH (2002). Systemic tumor-targeted gene delivery by anti-transferrin receptor scFv-immunoliposomes. *Mol Cancer Ther*. **1**:337–346.
- [7] Rait A, Pirolo KF, Xiang LM, Ulick D, Chang EH (2002). Tumor-targeting, systemically delivered antisense HER-2 chemosensitizes human breast cancer xenografts irrespective of HER-2 levels. *Mol Med*. **8**:476–487.
- [8] Rait A, Pirolo KF, Ulick D, Cullen K, Chang EH (2003). HER-2-targeted antisense oligonucleotides result in sensitization of head and neck cancer cells to chemotherapeutic agents. *Ann N Y Acad Sci*. **1002**:1–12.
- [9] Cristiano RJ, Curiel DT (1996). Strategies to accomplish gene delivery via the receptor-mediated endocytosis pathway. *Cancer Gene Ther*. **3**:49–57.
- [10] Cheng PW (1996). Receptor ligand-facilitated gene transfer: Enhancement of liposome-mediated gene transfer and expression by transferrin. *Hum Gene Ther*. **7**:275–282.
- [11] Keer HN, Kozlowski JM, Tsai YC, Lee C, McEwan RN, Grayhack JT (1990). Elevated transferrin receptor content in human prostate cancer cell lines assessed in vitro and in vivo. *J Urol*. **143**:381–385.
- [12] Rossi MC, Zetter BR (1992). Selective stimulation of prostatic carcinoma cell proliferation by transferrin. *Proc Natl Acad Sci USA*. **89**:6197–6201.
- [13] Elliott RL, Elliott MC, Wang F, Head JF (1993). Breast carcinoma and the role of iron metabolism. A cytochemical, tissue culture, and ultrastructural study. *Ann N Y Acad Sci*. **698**:159–166.
- [14] Thorstensen K, Romslo I (1993). The transferrin receptor: Its diagnostic value and its potential as therapeutic target. *Scand J Clin Lab Invest Suppl*. **215**:113–120.
- [15] Miyamoto T, Tanaka N, Eishi Y, Amagasa T (1994). Transferrin receptor in oral tumors. *Int J Oral Maxillofac Surg*. **23**:430–433.
- [16] Ponka P, Lok CN (1999). The transferrin receptor: Role in health and disease. *Int J Biochem Cell Biol*. **31**:1111–1137.

- [17] Haynes BF, Hemler M, Cotner T, Mann DL, Eisenbarth GS, Strominger JL, Fauci AS (1981). Characterization of a monoclonal antibody (5E9) that defines a human cell surface antigen of cell activation. *J Immunol.* **127**:347–351.
- [18] Batra JK, Fitzgerald DJ, Chaudhary VK, Pastan I (1991). Single-chain immunotoxins directed at the human transferrin receptor containing *Pseudomonas* exotoxin A or diphtheria toxin: Anti-TFR(Fv)-PE40 and DT388-anti-TFR(Fv). *Mol Cell Biol.* **11**:2200–2205.
- [19] Jain RK, Baxter LT (1988). Mechanisms of heterogenous distribution of monoclonal antibodies and other macro-molecules in tumors: Significance of elevated interstitial pressure. *Cancer Res.* **48**:7022–7032.
- [20] Wolfert MA, Schacht EH, Toncheva V, Ulbrich K, Nazarova O, Seymour LW (1996). Characterization of vectors for gene therapy formed by self-assembly of DNA with synthetic block copolymers. *Hum Gene Ther.* **7**:2123–2133.
- [21] Dunlap DD, Maggi A, Soria MR, Monaco L (1997). Nanoscopic structure of DNA condensed for gene delivery. *Nucleic Acids Res.* **25**:3095–3101.
- [22] Kawaura C, Noguchi A, Furuno T, Nakanishi M (1998). Atomic force microscopy for studying gene transfection mediated by cationic liposomes with a cationic cholesterol derivative. *FEBS Lett.* **421**:69–72.
- [23] Choi YH, Liu F, Choi JS, Kim SW, Park JS (1999). Characterization of a targeted gene carrier, lactose–polyethylene glycol-grafted poly-L-lysine and its complex with plasmid DNA. *Hum Gene Ther.* **10**:2657–2665.
- [24] Diebel CE, Proksch R, Green CR, Neilson P, Walker MM (2000). Magnetite defines a vertebrate magnetoreceptor. *Nature.* **406**:299–302.
- [25] Rasa M, Kuipers BWM, Philipse AP (2002). Atomic force microscopy and magnetic force microscopy study of model colloids. *J Colloid Interface Sci.* **250**:303–315.
- [26] Yu W, Pirollo KF, Yu B, Rait A, Xiang L, Huang W, Zhou Q, Ertem G, Chang EH (2004). Enhanced transfection efficiency of a systemically delivered tumor-targeting immunolipoplex by inclusion of a pH-sensitive histidylated oligolysine peptide. *Nucleic Acids Res.* **5**.
- [27] Alisaukus R, Wong GY, Gold DV (1995). Initial studies of monoclonal antibody PAM4 targeting to xenografted orthotopic pancreatic cancer. *Cancer Res.* **55**:5743s–5748s.
- [28] Foo JJ, Chan V, Liu KK (2003). Contact deformation of liposome in the presence of osmosis. *Ann Biomed Eng.* **31**:1279–1286.
- [29] Xu L, Frederick P, Pirollo K, Tang W, Rait A, Xiang L, Huang W-Q, Chang EH (2002). Self-assembly of a virus-mimicking nanostructure system for efficient tumor-targeted gene delivery. *Hum Gene Ther.* **13**:469–481.
- [30] Freedman M, Sarcone A, Pirollo KF, Lin C, Chang EH (2001). Ultrasound images of implanted tumors in nude mice using Sono-CT[®] correlated with MRI appearance. *SPIE Medical Imaging: Physiology and Function from Multidimensional Images.* **4321**:163–167.
- [31] Wisner ER, Weichert JP, Longino MA, Counsell RE, Weisbrode SE (2002). A surface-modified chylomicron remnant-like emulsion for percutaneous computed tomography lymphography: Synthesis and preliminary imaging findings. *Invest Radiol.* **37**:232–239.
- [32] Winter PM, Morawski AM, Caruthers SD, Fuhrhop RW, Zhang H, Williams TA, Allen JS, Lacy EK, Robertson JD, Lanza GM, Wickline SA (2003). Molecular imaging of angiogenesis in early-stage atherosclerosis with alpha(v)beta3-integrin-targeted nanoparticles. *Circulation.* **108**:2270–2274.
- [33] Morawski AM, Winter PM, Crowder KC, Caruthers SD, Fuhrhop RW, Scott MJ, Robertson JD, Abendschein DR, Lanza GM, Wickline SA (2004). Targeted nanoparticles for quantitative imaging of sparse molecular epitopes with MRI. *Magn Reson Med.* **51**:480–486.